

## 1 Fitting

### 1.1 Model: $\Lambda K_S^0$ , $\Lambda K^\pm$ , $\Xi^{ch} K_S^0$

The two-particle relative momentum correlation function may be written theoretically by the Koonin-Pratt equation [?, ?]:

$$C(\mathbf{k}^*) = \int S(\mathbf{r}^*) |\Psi_{\mathbf{k}^*}(\mathbf{r}^*)|^2 d^3 \mathbf{r}^* \quad (1)$$

In the absence of Coulomb effects, and assuming a spherically gaussian source of width  $R$ , the 1D femtoscopic correlation function can be calculated analytically using:

$$C(k^*) = 1 + C_{QI}(k^*) + C_{FSI}(k^*) \quad (2)$$

$C_{QI}$  describes plane-wave quantum interference:

$$C_{QI}(k^*) = \alpha \exp(-4k^{*2}R^2) \quad (3)$$

where  $\alpha = (-1)^{2j}/(2j+1)$  for identical particles with spin  $j$ , and  $\alpha = 0$  for non-identical particles. Obviously,  $\alpha = 0$  for all analyses presented in this note.  $C_{FSI}$  describes the s-wave strong final state interaction between the particles:

$$\begin{aligned} C_{FSI}(k^*) &= (1 + \alpha) \left[ \frac{1}{2} \left| \frac{f(k^*)}{R} \right|^2 \left( 1 - \frac{d_0}{2\sqrt{\pi}R} \right) + \frac{2\Re f(k^*)}{\sqrt{\pi}R} F_1(2k^*R) - \frac{\Im f(k^*)}{R} F_2(2k^*R) \right] \\ f(k^*) &= \left( \frac{1}{f_0} + \frac{1}{2} d_0 k^{*2} - ik^* \right)^{-1}; \quad F_1(z) = \int_0^z \frac{e^{x^2-z^2}}{z} dx; \quad F_2(z) = \frac{1-e^{-z^2}}{z} \end{aligned} \quad (4)$$

where  $R$  is the source size,  $f(k^*)$  is the s-wave scattering amplitude,  $f_0$  is the complex scattering length, and  $d_0$  is the effective range of the interaction.

An additional parameter  $\lambda$  is typically included in the femtoscopic fit function to account for the purity of the pair sample. In the case of no residual correlations (to be discussed in Section 1.4, the fit function becomes:

$$C(k^*) = 1 + \lambda [C_{QI}(k^*) + C_{FSI}(k^*)] \quad (5)$$

### 1.2 Model: $\Xi^{ch} K^{ch}$

The two-particle correlation function may be written as:

$$C(\mathbf{k}^*) = \sum_S \rho_S \int S(\mathbf{r}^*) |\Psi_{\mathbf{k}^*}^S(\mathbf{r}^*)|^2 d^3 \mathbf{r}^* \quad (6)$$

where  $\rho_S$  is the normalized emission probability of particles in a state with spin  $S$ ,  $S(\mathbf{r}^*)$  is the pair emission source distribution (assumed to be Gaussian), and  $\Psi_{\mathbf{k}^*}^S(\mathbf{r}^*)$  is the two-particle wave-function including both strong and Coulomb interactions [?]:

$$\Psi_{\mathbf{k}^*}(\mathbf{r}^*) = e^{i\delta_c} \sqrt{A_c(\eta)} [e^{i\mathbf{k}^*\cdot\mathbf{r}^*} F(-i\eta, 1, i\xi) + f_c(k^*) \frac{\tilde{G}(\rho, \eta)}{r^*}] \quad (7)$$

where  $\rho = k^* r^*$ ,  $\eta = (k^* a_c)^{-1}$ ,  $\xi = \mathbf{k}^* \cdot \mathbf{r}^* + k^* r^* \equiv \rho(1 + \cos \theta^*)$ , and  $a_c = (\mu z_1 z_2 e^2)^{-1}$  is the two-particle Bohr radius (including the sign of the interaction).  $\delta_c$  is the Coulomb s-wave phase shift,  $A_c(\eta)$  is the Coulomb penetration factor,  $\tilde{G} = \sqrt{A_c}(G_0 + iF_0)$  is a combination of the regular ( $F_0$ ) and singular ( $G_0$ ) s-wave Coulomb functions.  $f_c(k^*)$  is the s-wave scattering amplitude:

$$f_c(k^*) = \left[ \frac{1}{f_0} + \frac{1}{2} d_0 k^{*2} - \frac{2}{a_c} h(\eta) - ik^* A_c(\eta) \right]^{-1} \quad (8)$$

where, the “h-function”,  $h(\eta)$ , is expressed through the digamma function,  $\psi(z) = \Gamma'(z)/\Gamma(z)$  as:

$$h(\eta) = 0.5[\psi(i\eta) + \psi(-i\eta) - \ln(\eta^2)] \quad (9)$$

In this case, the  $\lambda$  parameter may be included as:

$$C(\mathbf{k}^*) = (1 - \lambda) + \lambda \sum_S \rho_S \int S(\mathbf{r}^*) |\Psi_{\mathbf{k}^*}^S(\mathbf{r}^*)|^2 d^3 \mathbf{r}^* \quad (10)$$

### 1.3 Momentum Resolution Corrections

Finite track momentum resolution causes the reconstructed momentum of a particle to smear around the true value. This, of course, also holds true for V0 particles. The effect is propagated up to the pairs of interest, which causes the reconstructed relative momentum ( $k_{Rec}^*$ ) to differ from the true momentum ( $k_{True}^*$ ). Smearing of the momentum typically will result in a suppression of the signal.

The effect of finite momentum resolution can be investigated using the MC data, for which both the true and reconstructed momenta are available. Figure 1 shows sample  $k_{True}^*$  vs.  $k_{Rec}^*$  plots for  $\Lambda(\bar{\Lambda})K^\pm$  0-10% analyses; Figure 1a was generated using same-event pairs, while Figure 1b was generated using mixed-event pairs (with  $N_{mix} = 5$ ).

If there are no contaminations in our particle collection, the plots in Figure 1 should be smeared around  $k_{True}^* = k_{Rec}^*$ ; this is mostly true in our analyses. However, there are some interesting features of our results which demonstrate a small (notice the log-scale on the z-axis) contamination in our particle collection. The structure around  $k_{Rec}^* = k_{True}^* - 0.15$  is mainly caused by  $K_S^0$  contamination in our  $\Lambda(\bar{\Lambda})$  sample. The remaining structure not distributed about  $k_{Rec}^* = k_{True}^*$  is due to  $\pi$  and  $e$  contamination in our  $K^\pm$  sample. These contaminations are more visible in Figure 2, which show  $k_{Rec}^*$  vs.  $k_{True}^*$  plots (for a small sample of the  $\Lambda K^\pm$  0-10% central analysis), for which the MC truth (i.e. true, known identity of the particle) was used to eliminate misidentified particles in the  $K^+(a)$  and  $\Lambda(b)$  collections. (NOTE: This is an old figure and is for a small sample of the data. A new version will be generated shortly. It, nonetheless, demonstrates the point well).

Information gained from looking at  $k_{Rec}^*$  vs  $k_{True}^*$  can be used to apply corrections to account for the effects of finite momentum resolution on the correlation functions. A typical method involves using the MC HIJING data to build two correlation functions,  $C_{Rec}(k^*)$  and  $C_{True}(k^*)$ , using the generator-level momentum ( $k_{True}^*$ ) and the measured detector-level momentum ( $k_{Rec}^*$ ). The data is then corrected by multiplying by the ratio,  $C_{True}/C_{Rec}$ , before fitting. This essentially unsmears the data, which can be compared directly to theoretical predictions and fits. Although this is conceptually simple, there are a couple of big disadvantages to this method. First, HIJING does not incorporate final-state interactions, so weights must be used when building same-event (numerator) distributions. These weights account for the interactions, and, in the absence of Coulomb interactions, can be calculated using Eq. 2. Of course, these weights are valid only for a particular set of fit parameters. Therefore, in the fitting process, during which the fitter explores a large parameter set, the corrections will not remain valid. As such, applying the momentum resolution correction and fitting becomes a long and drawn out iterative process. An initial

parameter set is obtained (through fitting without momentum resolution corrections, theoretical models, or a good guess), then the MC data is run over to obtain the correction factor, the data is fit using the correction factor, a refined parameter set is extracted, the MC data is run over again to obtain the new correction factor, etc. This process continues until the parameter set stabilizes. The second issue concerns statistics. With the MC data available on the grid, we were not able to generate the statistics necessary to use the raw  $C_{True}/C_{Rec}$  ratio. The ratio was not stable, and when applied to the data, obscured the signal. Attempting to fit the ratio to generate the corrections also proved problematic. However, as HIJING does not include final-state interactions, the same-event and mixed-event pairs are very similar (with the exception of things like energy and momentum conservation, etc). Therefore, one may build the numerator distribution using mixed-event pairs. This corresponds, more or less, to simply running a weight generator through the detector framework.

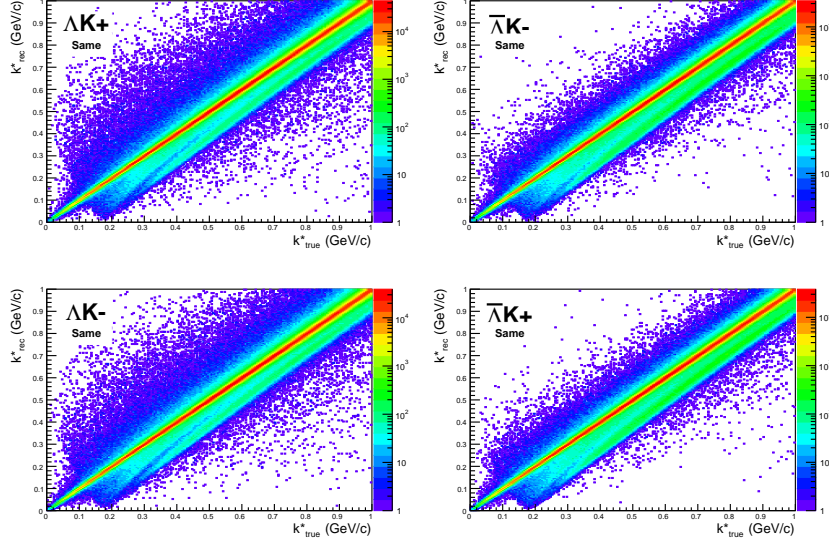
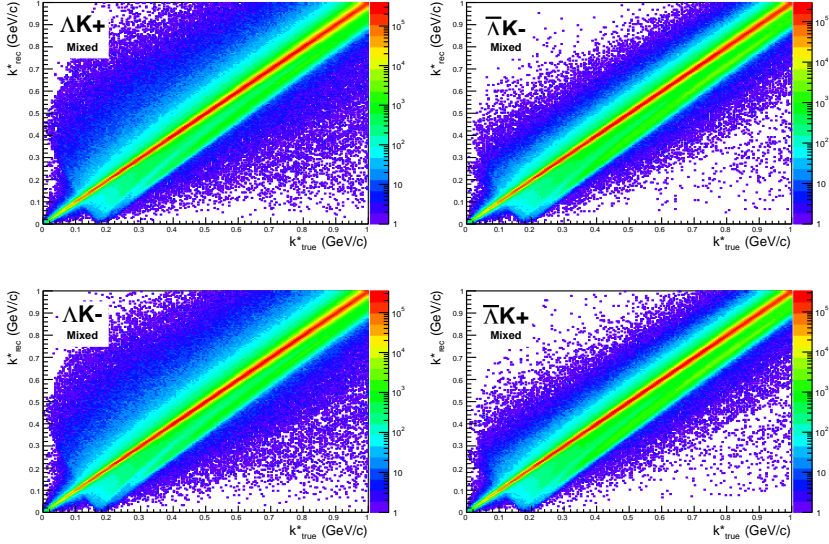
A second approach is to use information gained from plots like those in Figure 1, which can be considered response matrices. The response matrix describes quantitatively how each  $k_{Rec}^*$  bin receives contributions from multiple  $k_{True}^*$  bins, and can be used to account for the effects of finite momentum resolution. With this approach, the resolution correction is applied on-the-fly during the fitting process by propagating the theoretical (fit) correlation function through the response matrix, according to:

$$C_{fit}(k_{Rec}^*) = \frac{\sum_{k_{True}^*} M_{k_{Rec}^*, k_{True}^*} C_{fit}(k_{True}^*)}{\sum_{k_{True}^*} M_{k_{Rec}^*, k_{True}^*}} \quad (11)$$

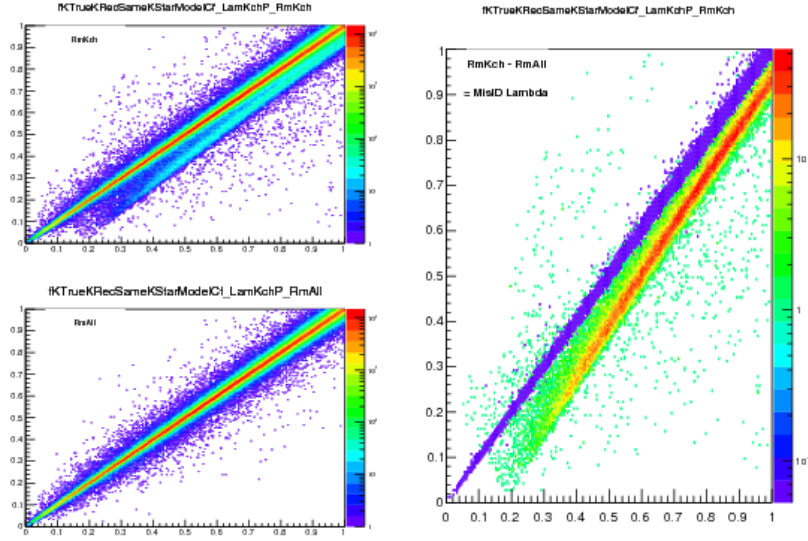
where  $M_{k_{Rec}^*, k_{True}^*}$  is the response matrix (Figure 1),  $C_{fit}(k_{True}^*)$  is the fit binned in  $k_{True}^*$ , and the denominator normalizes the result.

Equation 11 describes that, for a given  $k_{Rec}^*$  bin, the observed value of  $C(k_{Rec}^*)$  is a weighted average of all  $C(k_{True}^*)$  values, where the weights are the normalized number of counts in the  $[k_{Rec}^*, k_{True}^*]$  bin. As seen in Figure 1, overwhelmingly the main contributions come from the  $k_{Rec}^* = k_{True}^*$  bins. Although the correction is small, it is non-negligible for the low- $k^*$  region of the correlation function.

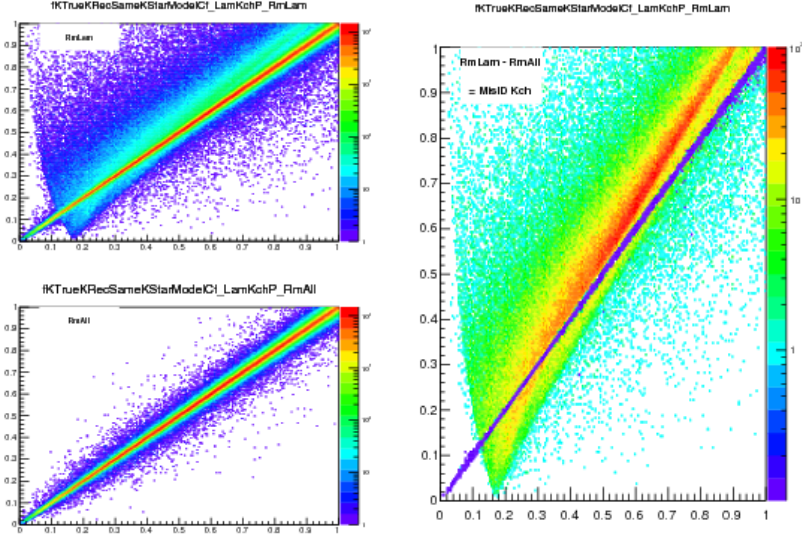
Here, the momentum resolution correction is applied to the fit, not the data. In other words, during fitting, the theoretical correlation function is smeared just as real data would be, instead of unsmeared the data. This may not be ideal for the theorist attempting to compare a model to experimental data, but it leaves the experimental data unadulterated. The current analyses use this second approach to applying momentum resolution corrections because of two major advantages. First, the MC data must be analyzed only once, and no assumptions about the fit are needed. Secondly, the momentum resolution correction is applied on-the-fly by the fitter, delegating the iterative process to a computer instead of the user.

(a) Same Event Pairs ( $\Lambda(\bar{\Lambda})K^\pm$ , 0-10% Centrality)(b) Mixed Event Pairs ( $\Lambda(\bar{\Lambda})K^\pm$ , 0-10% Centrality)

**Fig. 1:** Sample  $k_{True}^*$  vs.  $k_{Rec}^*$  plot for  $\Lambda(\bar{\Lambda})K^\pm$  0-10% analyses. The structure which appears around  $k_{Rec}^* = k_{True}^* - 0.15$  is mainly caused by  $K_S^0$  contamination in our  $\Lambda(\bar{\Lambda})$  sample. The remaining structure not distributed about  $k_{Rec}^* = k_{True}^*$  is due to  $\pi$  and  $e$  contamination in our  $K^\pm$  sample. These contaminations are more clearly visible in Figure 2



(a) (Top Left) All misidentified  $K^+$  excluded. (Bottom Left) All misidentified  $\Lambda$  and  $K^+$  excluded. (Right) The difference of (Top Left) - (Bottom Left), which reveals the contamination in our  $\Lambda$  collection. The structure which appears around  $k_{Rec}^* = k_{True}^* - 0.15$  is mainly caused by  $K_S^0$  contamination in our  $\Lambda(\bar{\Lambda})$  sample.



(b) (Top Left) All misidentified  $\Lambda$  excluded. (Bottom Left) All misidentified  $\Lambda$  and  $K^+$  excluded. (Right) The difference of (Top Left) - (Bottom Left), which reveals the contamination in our  $K^+$  collection. The structure not distributed about  $k_{Rec}^* = k_{True}^*$  is due to  $\pi$  and  $e^-$  contamination in our  $K^+$  sample.

**Fig. 2:** Note: This is an old figure and is for a small sample of the data. A new version will be generated shortly.  
y-axis =  $k_{Rec}^*$ , x-axis =  $k_{True}^*$ .

(Left)  $k_{Rec}^*$  vs.  $k_{True}^*$  plots for a small sample of the  $\Lambda K^+$  0-10% central analysis, MC truth was used to eliminate misidentified particles in the  $K^+$ (a) and  $\Lambda$ (b) collections. (Right) The difference of the top left and bottom left plots. Contaminations in our particle collections are clearly visible. Figure (a) demonstrates a  $K_S^0$  contamination in our  $\Lambda$  collection; Figure (b) demonstrates a  $\pi$  and  $e^-$  contamination in our  $K^\pm$  collection.

## 1.4 Residual Correlations

The purpose of this analysis is study the interaction and scale of the emitting source of the pairs. In order to obtain correct results, it is important for our particle collections to consist of primary particles. In practice, this is difficult to achieve for our  $\Lambda$  and  $\bar{\Lambda}$  collections. Many of our  $\Lambda$  particles are not primary, but originate as decay products from other hyperons, including  $\Sigma^0$ ,  $\Xi^0$ ,  $\Xi^-$  and  $\Sigma^{*(+,-,0)}(1385)$ . Additionally, many of our K particles are not primary, but decay from  $K^{*(+,-,0)}(892)$  parents. In these decays, the  $\Lambda$  carries away a momentum very similar to that of its parent. As a result, the correlation function between a secondary  $\Lambda$  and, for instance, a  $K^+$  will be sensitive to, and dependent upon, the interaction between the parent of the  $\Lambda$  and the  $K^+$ . In effect, the correlation between the parent of the  $\Lambda$  and the  $K^+$  (ex.  $\Sigma^0 K^+$ ) will be visible, although smeared out, in the  $\Lambda K^+$  data. We call this a residual correlation resulting from feed-down. Residual correlations are important in an analysis when three criteria are met [?]: i) the parent correlation signal is large, ii) a large fraction of pairs in the sample originate from the particular parent system, and iii) the decay momenta are comparable to the expected correlation width in  $k^*$ .

As it is difficult for us to eliminate these residual correlations in our analyses, we must attempt to account for them in our fitter. To achieve this, we will simultaneously fit the data for both the primary correlation function and the residual correlations. For example, in the simple case of a  $\Lambda K^+$  analysis with residuals arising solely from  $\Sigma^0 K^+$  feed-down:

$$C_{measured}(k_{\Lambda K^+}^*) = 1 + \lambda_{\Lambda K^+}[C_{\Lambda K^+}(k_{\Lambda K^+}^*) - 1] + \lambda_{\Sigma^0 K^+}[C_{\Sigma^0 K^+}(k_{\Lambda K^+}^*) - 1]$$

$$C_{\Sigma^0 K^+}(k_{\Lambda K^+}^*) \equiv \frac{\sum_{k_{\Sigma^0 K^+}^*} C_{\Sigma^0 K^+}(k_{\Sigma^0 K^+}^*) T(k_{\Sigma^0 K^+}^*, k_{\Lambda K^+}^*)}{\sum_{k_{\Sigma^0 K^+}^*} T(k_{\Sigma^0 K^+}^*, k_{\Lambda K^+}^*)} \quad (12)$$

$C_{\Sigma^0 K^+}(k_{\Sigma^0 K^+}^*)$  is the  $\Sigma^0 K^+$  correlation function from, for instance, Equation 2, and  $T$  is the transform matrix generated with THERMINATOR. The transform matrix is formed for a given parent pair, AB, by taking all  $\Lambda K$  pairs originating from AB, calculating the relative momentum of the parents ( $k_{AB}^*$ ) and daughters ( $k_{\Lambda K}^*$ ), and filling a two-dimensional histogram with the values. The transform matrix is essentially an unnormalized probability distribution mapping the  $k^*$  of the parent pair to that of the daughter pair when one or both parents decay. An example of such transform matrices can be found in Figures 3 and 4.

The above equation can be easily extended to include feed-down from more sources:

$$C_{measured}(k_{\Lambda K}^*) = 1 + \lambda_{\Lambda K}[C_{\Lambda K}(k_{\Lambda K}^*) - 1] + \lambda_{\Sigma^0 K}[C_{\Sigma^0 K}(k_{\Lambda K}^*) - 1] + \dots$$

$$+ \lambda_{P_1 P_2}[C_{P_1 P_2}(k_{\Lambda K}^*) - 1] + \lambda_{other}[C_{other}(k_{\Lambda K}^*) - 1]$$

$$C_{P_1 P_2}(k_{\Lambda K}^*) \equiv \frac{\sum_{k_{P_1 P_2}^*} C_{P_1 P_2}(k_{P_1 P_2}^*) T(k_{P_1 P_2}^*, k_{\Lambda K}^*)}{\sum_{k_{P_1 P_2}^*} T(k_{P_1 P_2}^*, k_{\Lambda K}^*)} \quad (13)$$

Or, more compactly:

$$C_{measured}(k_{\Lambda K}^*) = 1 + \sum_i \lambda_i [C_i(k_{\Lambda K}^*) - 1] \quad (14)$$

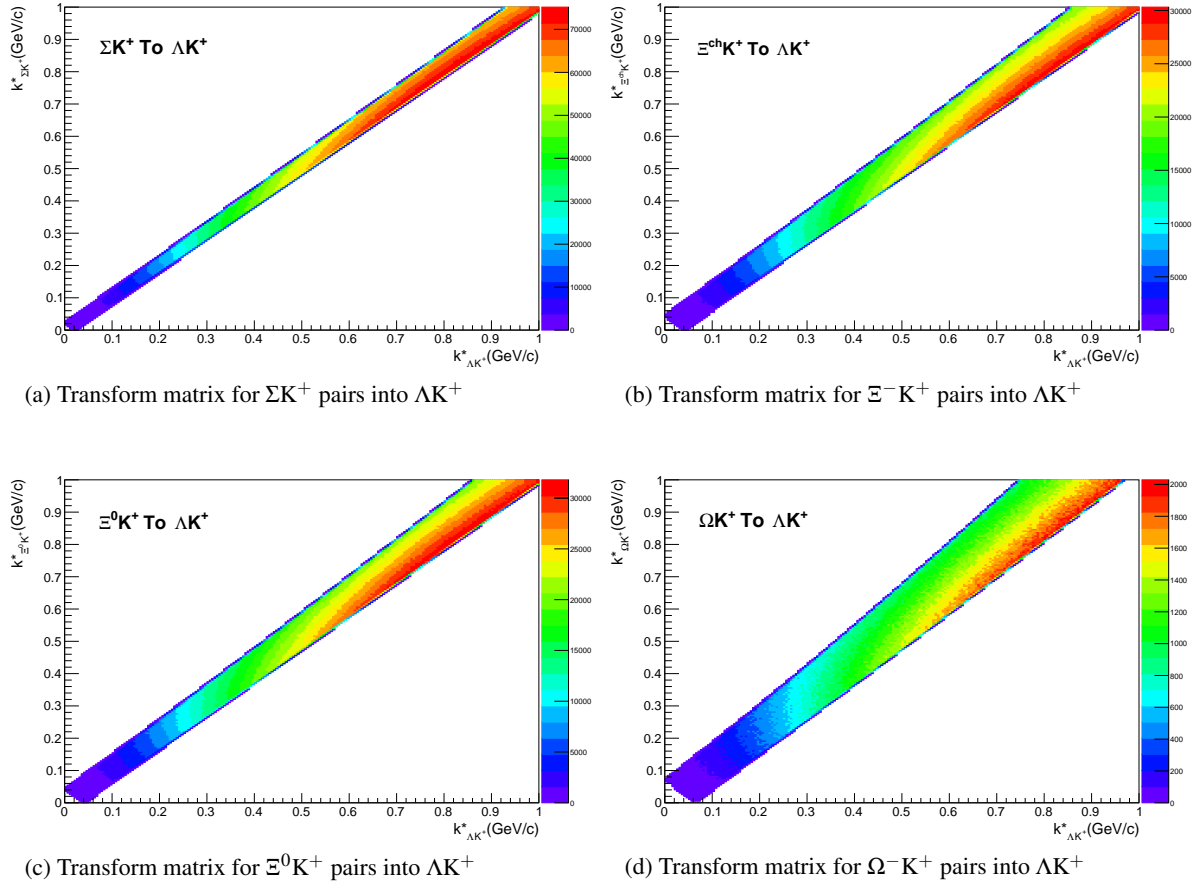


**Fig. 3:** Transform Matrices generated with THERMINATOR for  $\Lambda K^+$  Analysis

So, in practice, we model the correlation function of the parents, and run the correlation function through the appropriate transform matrix to determine the contribution to the daughter correlation function. A few questions still remain. First, what  $\lambda$  values should be used in the above equation? One option would be to leave all of these  $\lambda$ -parameters free during the fit process. However, this would introduce a huge number of new parameters into the fitter, and would make the fit results less trustworthy. The  $\lambda$  parameters roughly dictate the strength of the parent contribution to the daughter pair. Additionally, as found in [?], the reconstruction efficiency for primary  $\Lambda$  particles is nearly equal to that of  $\Lambda$  particles originating from  $\Sigma$ ,  $\Sigma^*$ ,  $\Xi^0$ ,  $\Xi^-$ , and  $\Omega$  hyperons. Therefore, the  $\lambda$  parameter for parent system AB can be estimated using THERMINATOR as the total number of  $\Lambda K$  pairs originating from AB ( $N_{AB}$ ) divided by the total number of  $\Lambda K$  pairs ( $N_{Total}$ ):

$$\lambda_{AB} = \frac{N_{AB}}{N_{Total}} \quad (15)$$

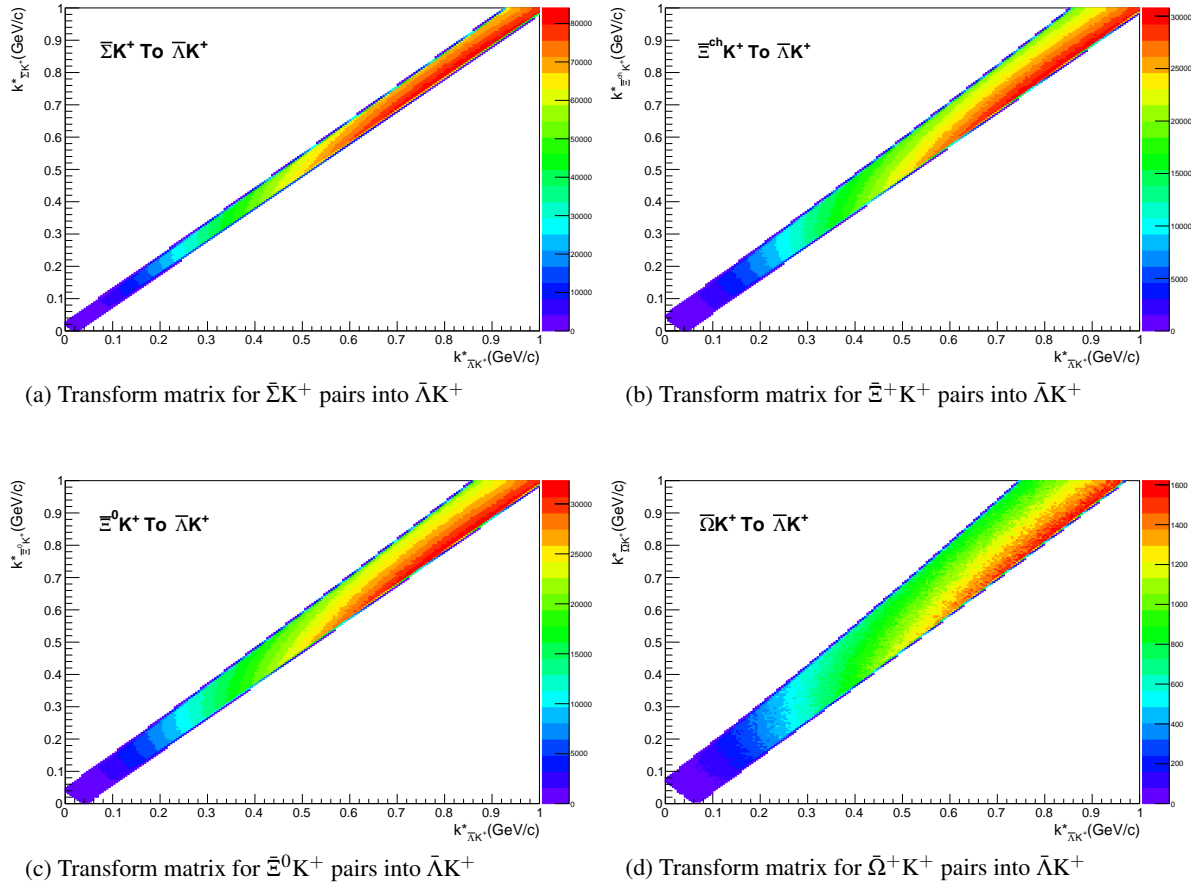


**Fig. 4:** Transform Matrices generated with THERMINATOR for  $\bar{\Lambda}K^+$  Analysis

AK <sup>+</sup> Residuals		ĀK <sup>-</sup> Residuals	
Pair System	λ value	Pair System	λ value
ΛK <sup>+</sup>	0.154	ĀK <sup>-</sup>	0.158
Σ <sup>0</sup> K <sup>+</sup>	0.099	ĀΣ <sup>0</sup> K <sup>-</sup>	0.102
Ξ <sup>0</sup> K <sup>+</sup>	0.072	ĀΞ <sup>0</sup> K <sup>-</sup>	0.067
Ξ <sup>-</sup> K <sup>+</sup>	0.069	ĀΞ <sup>+</sup> K <sup>-</sup>	0.065
Other	0.558	Other	0.560
Fakes	0.048	Fakes	0.048

**Table 1:**  $\lambda$  values for the individual components of the  $\Lambda K^+$  (left) and  $\bar{\Lambda} K^-$  (right) correlation functions for the case of 3 residual contributions.

AK <sup>+</sup> Residuals		ĀK <sup>-</sup> Residuals	
Pair System	λ value	Pair System	λ value
ΛK <sup>+</sup>	0.154	ĀK <sup>-</sup>	0.158
Σ <sup>0</sup> K <sup>+</sup>	0.099	ĀΣ <sup>0</sup> K <sup>-</sup>	0.102
Ξ <sup>0</sup> K <sup>+</sup>	0.072	ĀΞ <sup>0</sup> K <sup>-</sup>	0.067
Ξ <sup>-</sup> K <sup>+</sup>	0.069	ĀΞ <sup>+</sup> K <sup>-</sup>	0.065
Σ <sup>*+</sup> K <sup>+</sup>	0.046	ĀΣ <sup>*-</sup> K <sup>-</sup>	0.046
Σ <sup>*-</sup> K <sup>+</sup>	0.042	ĀΣ <sup>*+</sup> K <sup>-</sup>	0.045
Σ <sup>*0</sup> K <sup>+</sup>	0.042	ĀΣ <sup>*0</sup> K <sup>-</sup>	0.040
ΛK <sup>*0</sup>	0.039	ĀΛK <sup>*0</sup>	0.041
Σ <sup>0</sup> K <sup>*0</sup>	0.035	ĀΣ <sup>0</sup> K <sup>*0</sup>	0.036
Ξ <sup>0</sup> K <sup>*0</sup>	0.025	ĀΞ <sup>0</sup> K <sup>*0</sup>	0.024
Ξ <sup>-</sup> K <sup>*0</sup>	0.024	ĀΞ <sup>+</sup> K <sup>*0</sup>	0.023
Other	0.305	Other	0.305
Fakes	0.048	Fakes	0.048

**Table 2:**  $\lambda$  values for the individual components of the  $\Lambda K^+$  (left) and  $\bar{\Lambda} K^-$  (right) correlation functions for the case of 10 residual contributions.

$\Lambda K^-$ Residuals		$\bar{\Lambda} K^+$ Residuals	
Pair System	$\lambda$ value	Pair System	$\lambda$ value
$\Lambda K^-$	0.154	$\bar{\Lambda} K^+$	0.158
$\Sigma^0 K^-$	0.099	$\bar{\Sigma}^0 K^+$	0.103
$\Xi^0 K^-$	0.071	$\bar{\Xi}^0 K^+$	0.068
$\Xi^- K^-$	0.068	$\bar{\Xi}^+ K^+$	0.066
Other	0.561	Other	0.557
Fakes	0.048	Fakes	0.048

**Table 3:**  $\lambda$  values for the individual components of the  $\Lambda K^-$  (left) and  $\bar{\Lambda} K^+$  (right) correlation functions for the case of 3 residual contributions.

$\Lambda K^-$ Residuals		$\bar{\Lambda} K^+$ Residuals	
Pair System	$\lambda$ value	Pair System	$\lambda$ value
$\Lambda K^-$	0.154	$\bar{\Lambda} K^+$	0.158
$\Sigma^0 K^-$	0.099	$\bar{\Sigma}^0 K^+$	0.103
$\Xi^0 K^-$	0.071	$\bar{\Xi}^0 K^+$	0.068
$\Xi^- K^-$	0.068	$\bar{\Xi}^+ K^+$	0.066
$\Sigma^{*+} K^-$	0.046	$\bar{\Sigma}^{*-} K^+$	0.046
$\Sigma^{*-} K^-$	0.041	$\bar{\Sigma}^{*+} K^+$	0.045
$\Sigma^{*0} K^-$	0.041	$\bar{\Sigma}^{*0} K^+$	0.041
$\Lambda \bar{K}^{*0}$	0.039	$\bar{\Lambda} K^{*0}$	0.041
$\Sigma^0 \bar{K}^{*0}$	0.035	$\bar{\Sigma}^0 K^{*0}$	0.036
$\Xi^0 \bar{K}^{*0}$	0.025	$\bar{\Xi}^0 K^{*0}$	0.024
$\Xi^- \bar{K}^{*0}$	0.024	$\bar{\Xi}^+ K^{*0}$	0.023
Other	0.308	Other	0.301
Fakes	0.048	Fakes	0.048

**Table 4:**  $\lambda$  values for the individual components of the  $\Lambda K^-$  (left) and  $\bar{\Lambda} K^+$  (right) correlation functions for the case of 10 residual contributions.

$\Lambda K_S^0$ Residuals		$\bar{\Lambda} K_S^0$ Residuals	
Pair System	$\lambda$ value	Pair System	$\lambda$ value
$\Lambda K_S^0$	0.165	$\bar{\Lambda} K_S^0$	0.169
$\Sigma^0 K_S^0$	0.107	$\bar{\Sigma}^0 K_S^0$	0.111
$\Xi^0 K_S^0$	0.077	$\bar{\Xi}^0 K_S^0$	0.073
$\Xi^- K_S^0$	0.075	$\bar{\Xi}^+ K_S^0$	0.071
Other	0.528	Other	0.528
Fakes	0.048	Fakes	0.048

**Table 5:**  $\lambda$  values for the individual components of the  $\Lambda K_S^0$  (left) and  $\bar{\Lambda} K_S^0$  (right) correlation functions for the case of 3 residual contributions.

$\Lambda K_S^0$ Residuals		$\bar{\Lambda} K_S^0$ Residuals	
Pair System	$\lambda$ value	Pair System	$\lambda$ value
$\Lambda K_S^0$	0.165	$\bar{\Lambda} K_S^0$	0.169
$\Sigma^0 K_S^0$	0.107	$\bar{\Sigma}^0 K_S^0$	0.111
$\Xi^0 K_S^0$	0.077	$\bar{\Xi}^0 K_S^0$	0.073
$\Xi^- K_S^0$	0.075	$\bar{\Xi}^+ K_S^0$	0.071
$\Sigma^{*+} K_S^0$	0.050	$\bar{\Sigma}^{*-} K_S^0$	0.050
$\Sigma^{*-} K_S^0$	0.045	$\bar{\Sigma}^{*+} K_S^0$	0.049
$\Sigma^{*0} K_S^0$	0.045	$\bar{\Sigma}^{*0} K_S^0$	0.044
$\Lambda K^{*0}$	0.019	$\bar{\Lambda} K^{*0}$	0.020
$\Sigma^0 K^{*0}$	0.017	$\bar{\Sigma}^0 K^{*0}$	0.017
$\Xi^0 K^{*0}$	0.012	$\bar{\Xi}^0 K^{*0}$	0.011
$\Xi^- K^{*0}$	0.012	$\bar{\Xi}^+ K^{*0}$	0.011
Other	0.329	Other	0.326
Fakes	0.048	Fakes	0.048

**Table 6:**  $\lambda$  values for the individual components of the  $\Lambda K_S^0$  (left) and  $\bar{\Lambda} K_S^0$  (right) correlation functions for the case of 10 residual contributions.

Now, the remaining question is how do we model the parent correlation functions? In an ideal world, we would simply look up the parent interaction in some table, and input this into our Lednicky equation (for the case of one or more charge neutral particle in the pair), or run it through the CoulombFitter machinery described in Sec. 1.2. Unfortunately, the world in which we live is not perfect, such a table does not exists, and little is known about the interaction between the residual pairs in this study. One solution would be to introduce a set of scattering parameters and radii for each residual system. However, as will the case of the  $\lambda$ -parameters above, this would introduce a large number of additional fit parameters, and would make our fitter too unconstrained and would yield untrustworthy results. The second option, which is adopted in this analysis, is to assume all residual pairs have the same source size as the daughter pair, and all Coulomb-neutral residual pairs also share the same scattering parameters as the daughter pair (the case of charged pairs will be described below).

Concerning the radii of the residual parent pairs, it was suggested that these should be set to smaller values. In the interest of minimizing the number of parameters in the fitter, we tested this by introducing an  $m_T$ -scaling of the parent radii. The motivation for this scaling comes from the approximate  $m_T$ -scaling of the radii observed in ???. To achieve this scaling, we assume the radii follow an inverse-square-root distribution:  $R_{AB} = \alpha m_T^{-1/2}$ . Then, it follows that we should scale the parent radii as:

$$R_{AB} = R_{\Lambda K} \left( \frac{m_{T,AB}}{m_{T,\Lambda K}} \right)^{-1/2} \quad (16)$$

The values for  $m_T$  for each pair system was taken from THERMINATOR. As the fitter dances around parameter space and selects new radii for the  $\Lambda K$  pairs, the radii of the residuals is scaled by the above factor. In the end, this scaling factor made no significant difference in our fit results, so this complication is excluded from our final results. Note that this is not surprising, as the most extreme scaling factor was, in the case of using 10 residual systems, between  $\Lambda K^+$  with  $m_{T,\Lambda K^+} \approx 1.4 \text{ GeV}/c^2$  and  $\Xi^- K^{*0}$  with  $m_{T,\Xi^- K^{*0}} \approx 1.8 \text{ GeV}/c^2$ , resulting in a scale factor of  $\approx 0.9$ .

Now, as hinted above, accounting for charged residuals adds a complication in that they necessitate the inclusion of the CoulombFitter into the process. The complication of combining the two fitters is not troubling, but it increases the fitting time drastically (the parallelization of the CoulombFitter across a large number of GPU cores, to drastically decrease run-time, is currently underway). We have two solutions to bypass such a large increase in run time. First, we can use our experimental  $\Xi^{\text{ch}} K^{\text{ch}}$  data to represent all charged parent pair system. In this case, there is no need to make any assumption about scattering parameters or source sizes, as we already have the experimental data. The downside is that, especially in the 30-50% centrality bin, the error bars on the data are large. Alternatively, we can assume the strong interaction is negligible in the charged residual, and generate the parent correlation function given radius and  $\lambda$  parameters. We find in our  $\Xi^{\text{ch}} K^{\text{ch}}$  study that a Coulomb-only description of the system describes, reasonably well, the broad features of the correlation. The strong interaction is necessary for the fine details. However, as these correlations are run through a transform matrix, which largely flattens out and fine details, a Coulomb-only description should be sufficient. In practice, this Coulomb-only scenario is achieved by first building a large number of Coulomb-only correlations for various radii and  $\lambda$  parameter values, and interpolating from this grid during the fitting process. We find consistent results between using the  $\Xi K$  data and the Coulomb-only interpolation method. When the number of residual pairs used is increased to 10, so that pairs such as  $\Sigma^{*+} K^-$  enter the picture, the Coulomb-only interpolation method is used. In other words, the  $\Xi K$  experimental data is only used to model the  $\Xi K$  residual contribution, all other charged pairs are treated with the Coulomb-only interpolation method.

Two examples of how very different transform matrices can alter a correlation function are shown in Figures 5 and 6 below. These figures were taken using parameter values obtained from fits to the data. In the top left corner of the figures, the input correlation function (closed symbols) is shown together with the output, transformed, correlation function (open symbols). In the bottom left, the transformed correlation is shown by itself. This is especially helpful when the  $\lambda$  parameter is very small, in which case the contribution in the top left can look flat, but the zoomed in view in the bottom left shows the structure. The right two plots in each figure show the transform matrix without (top right) and with (bottom right) a log-scale on the z-axis. Note, more examples of these transforms can be found in Sec. ??.

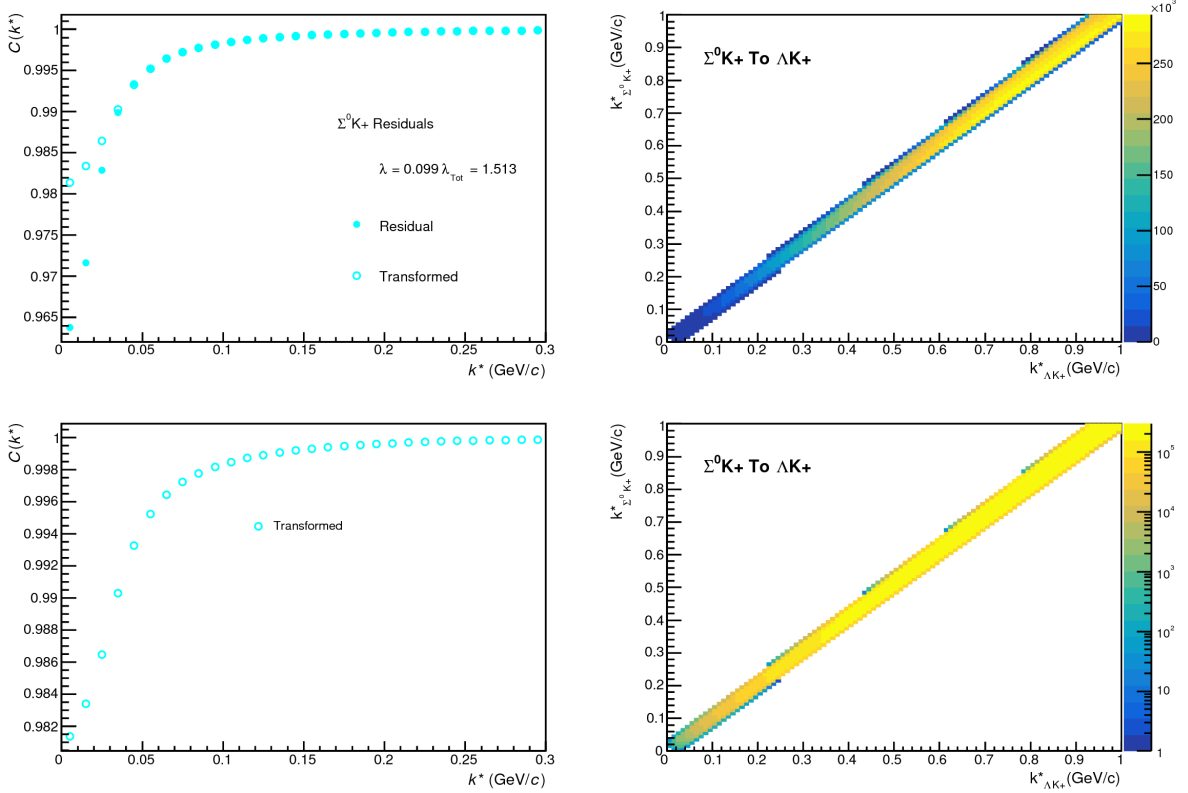


**Fig. 5:**  $\Sigma^0 K^+$  Transform. These figures were taken using parameter values obtained from fits to the data. In the top left corner of the figures, the input correlation function (closed symbols) is shown together with the output, transformed, correlation function (open symbols). In the bottom left, the transformed correlation is shown by itself. The right two plots in each figure show the transform matrix without (top right) and with (bottom right) a log-scale on the z-axis.

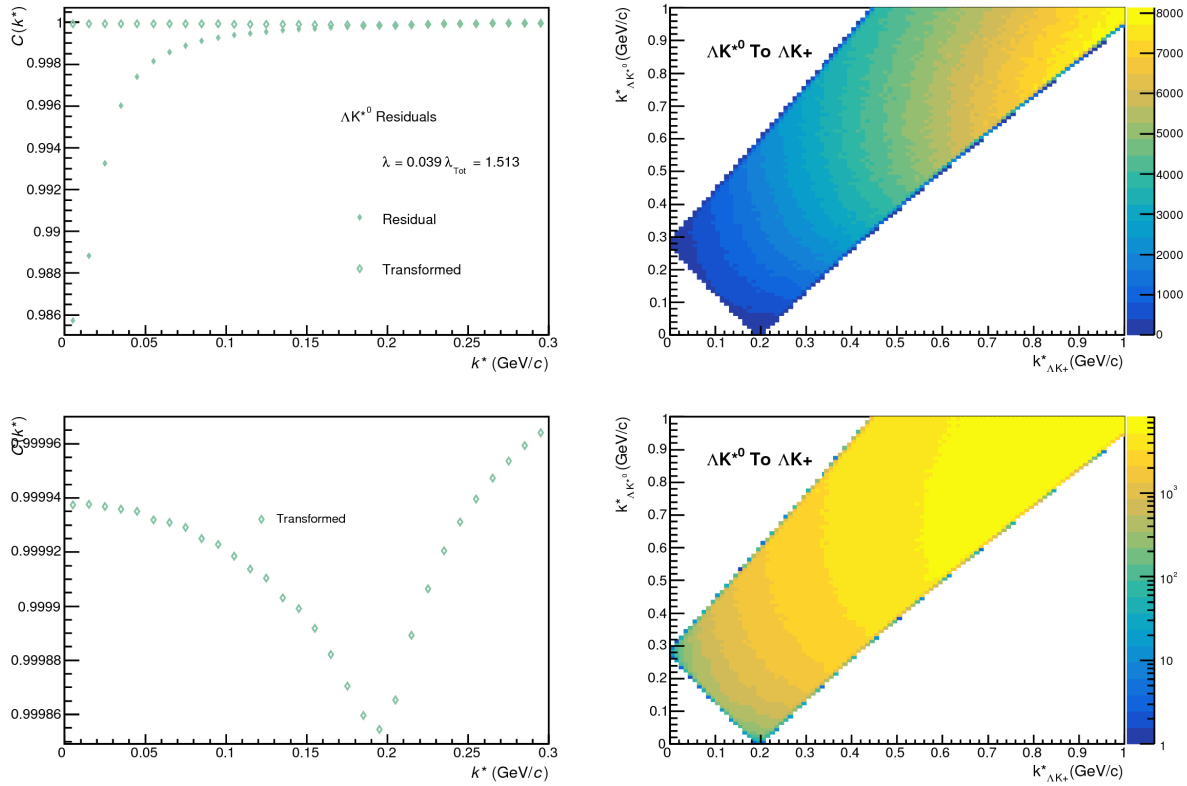


**Fig. 6:**  $\Sigma^0 K^+$  Transform. These figures were taken using parameter values obtained from fits to the data. In the top left corner of the figures, the input correlation function (closed symbols) is shown together with the output, transformed, correlation function (open symbols). In the bottom left, the transformed correlation is shown by itself. The right two plots in each figure show the transform matrix without (top right) and with (bottom right) a log-scale on the z-axis.

## 1.5 Non-Flat Background

Non-flat background

## 1.6 LednickyFitter

The code developed to fit the data is called “LednickyFitter”, and utilizes the ROOT TMinuit implementation of the MINUIT fitting package. In short, given a function with a number of parameters, the fitter explores the parameter space searching for the minimum of the equation. In this implementation, the function to be minimized should represent the difference between the measure and theoretical correlation functions. However, a simple  $\chi^2$  test is inappropriate for fitting correlation functions, as the ratio two Poisson distributions does not result in a Poisson distribution. Instead, a log-likelihood fit function of the following form is used [?]:

$$\chi_{PML}^2 = -2 \left[ A \ln \left( \frac{C(A+B)}{A(C+1)} \right) + B \ln \left( \frac{A+B}{B(C+1)} \right) \right] \quad (17)$$

where  $A$  is the experimental signal distribution (numerator),  $B$  is the experimental background distribution (denominator), and  $C$  is the theoretical fit correlation function.

The LednickyFitter uses Equations 2 – 4 to build the theoretical fit, and Equation 17 as the statistic quantifying the quality of the fit. The parameters to be varied by MINUIT are:  $\lambda$ ,  $R$ ,  $f_0$  ( $\mathbb{R}f_0$  and  $\mathbb{I}f_0$  separately),  $d_0$ , and normalization  $N$ . The fitter currently includes methods to correct for momentum resolution and a non-flat background. These corrections are applied to the fit function, the data is never touched. The fitter is able to share parameters between different analyses and fit all simultaneously.

In a typical fit, a given pair is fit with its conjugate (ex.  $\Lambda K^+$  with  $\bar{\Lambda} K^-$ ) across all centralities (0-10%, 10-30%, 30-50%), for a total of 6 simultaneous analyses. Each analysis has a unique  $\lambda$  and normalization parameter. The radii are shared between analyses of like centrality, as these should have similar source sizes. The scattering parameters ( $\mathbb{R}f_0$ ,  $\mathbb{I}f_0$ ,  $d_0$ ) are shared amongst all.

In the case of fitting with residuals, the  $\lambda_{Fit}$  parameter serves as an overall normalization shared by all contributors, such that Eqn 14 becomes:

$$\begin{aligned} C_{measured}(k_{\Lambda K}^*) &= 1 + \sum_i \lambda'_i [C_i(k_{\Lambda K}^*) - 1] \\ \lambda'_i &= \lambda_{Fit} \lambda_i \\ \sum_i \lambda'_i &= \lambda_{Fit} \sum_i \lambda_i = \lambda_{Fit} \end{aligned} \quad (18)$$

where  $\lambda_i$  is obtained from THERMINATOR, as explained in Section 1.4, and whose values are presented in Tables 1 through 6. For Coulomb-neutral pairs, such as  $\Lambda K$ ,  $\Sigma^0 K$ , and  $\Xi^0 K$ ,  $C_i(k_{\Lambda K}^*)$  is calculated from Eqn. 2, with the help of Eqn. 4. For those residual pairs which include a Coulomb interaction,  $C_i(k_{\Lambda K}^*)$  is either calculated using the CoulombFitter method (Sections 1.2 and 1.7) with no strong interaction, or by using the  $\Xi^{ch} K^{ch}$  data directly. Unless otherwise stated, the  $\Xi^{ch} K^{ch}$  residual contribution is modeled using the experimental  $\Xi^{ch} K^{ch}$  data, and all other charged contributors (ex.  $\Sigma^{*ch} K^{ch}$ ) are modeled using the CoulombFitter technique with no strong interaction contribution.

To summarize, the complete fit function is constructed as follows:

1. The uncorrected correlation function,  $C'_{Fit}(k_{True}^*)$ , is constructed using Eq. 19

- in the case of no residual contributions included in the fit,  $\lambda_i = \lambda_{\Lambda K}$  in Eq. 19 is set equal to 1. Then, the extracted  $\lambda_{Fit}$  parameter should be roughly equal to the pair purity.

2. The correlation function is corrected to account for momentum resolution effects using Eq. 11

$$- C'_{fit}(k^*_{Rec}) = \frac{\sum_{k^*_{True}} M_{k^*_{Rec}, k^*_{True}} C'_{fit}(k^*_{True})}{\sum_{k^*_{True}} M_{k^*_{Rec}, k^*_{True}}}$$

3. Finally, the non-flat background correction is applied, and the final fit function is obtained

$$- C_{Fit}(k^*_{Rec}) = C'_{Fit}(k^*_{Rec}) * F_{Bgd}(k^*_{Rec})$$

Figures ??, ??, and ?? (??, ??, and ??, or ??, ??, and ??), in Section ??, show experimental data with fits for all studied centralities for  $\Lambda K_S^0$  with  $\bar{\Lambda} K_S^0$ ,  $\Lambda K^+$  with  $\bar{\Lambda} K^-$ , and  $\Lambda K^-$  with  $\bar{\Lambda} K^+$ , respectively. In the figures, the black solid line represents the “raw” fit, i.e. not corrected for momentum resolution effects nor non-flat background. The green line shows the fit to the non-flat background. The purple points show the fit after momentum resolution, non-flat background, and residual correlations (if applicable) corrections have been applied. The initial values of the parameters is listed, as well as the final fit values with uncertainties.

## 1.7 Coulomb Fitter

When fitting the  $\Xi^-(\bar{\Xi}^+)K^\pm$  results, it is necessary to include both strong and Coulomb effects. In this case, Equation 2 is no longer valid, and, in fact, there is no analytical form with which to fit. Therefore, we must begin with the wave function describing the pair interaction, and simulate many particle pairs to obtain a theoretical fit correlation function. The code developed to achieve this functionality is called “CoulombFitter”. Currently, in order to generate the statistics needed for a stable fit, we find that  $\sim 10^4$  simulated pairs per 10 MeV bin are necessary. Unfortunately, the nature of this process means that the “CoulombFitter” takes much longer to run than the “LednickyFitter” of Section 1.1.

Unfortunately, with this analysis, we are not sensitive to, and therefore not able to distinguish between, the iso-spin singlet and triplet states. We proceed with our analysis, but the results must be interpreted as iso-spin averaged scattering parameters.

As stated before, to generate a fit correlation function, we must simulate a large number of pairs, calculate the wave-function, and average  $\Psi^2$  over all pairs in a given  $k^*$  bin. Essentially, we calculate Equation 6 by hand:

$$\begin{aligned} C(\mathbf{k}^*) &= \sum_S \rho_S \int S(\mathbf{r}^*) |\Psi_{\mathbf{k}^*}^S(\mathbf{r}^*)|^2 d^3 \mathbf{r}^* \\ &\longrightarrow C(|\mathbf{k}^*|) \equiv C(k^*) = \sum_S \rho_S \langle |\Psi^S(\mathbf{k}_i^*, \mathbf{r}_i^*)|^2 \rangle_i \\ &\longrightarrow C(k^*) = \lambda \sum_S \rho_S \langle |\Psi^S(\mathbf{k}_i^*, \mathbf{r}_i^*)|^2 \rangle_i + (1 - \lambda) \end{aligned} \quad (19)$$

where  $\langle \rangle_i$  represents an average over all pairs in a given  $k^*$  bin.

In summary, for a given  $k^*$  bin, we must draw  $N_{pairs} \sim 10^4$  pairs, and for each pair:

1. Draw a random  $\mathbf{r}^*$  vector according to our Gaussian source distribution  $S(\mathbf{r}^*)$
2. Draw a random  $\mathbf{k}^*$  vector satisfying the  $|\mathbf{k}^*|$  restriction of the bin

- 
- We draw from real  $k^*$  vectors obtained from the data
  - However, we find that drawing from a distribution flat in  $k^*$  gives similar results

### 3. Construct the wave-function $\Psi$

After all pairs for a given  $k^*$  bin are simulated and wave-functions obtained, the results are averaged to give the fit result.

Construction of the wave-functions, Equation 7, involves a number of complex functions not included in standard C++ or ROOT libraries (namely,  $h(\eta)$ ,  $\tilde{G}(\rho, \eta)$ ), and  $F(-i\eta, 1, i\xi)$ . These functions were even difficult to find and implement from elsewhere. Our solution was to embed a Mathematica kernel into our C++ code to evaluate these functions. However, having Mathematica work on-the-fly with the fitter was far too time consuming (fitter would have taken day, maybe weeks to finish). Our solution was to use Mathematica to create matrices representing these functions for different parameter values. During fitting, these matrices were then interpolated and the results used to build the wave-functions. This method decreased the running time dramatically, and we are not able to generate results in under  $\sim 1$  hour. This process will be explained in more detail in future versions of the note.